JOURNAL OF MATERIALS SCIENCE 30 (1995) 2877–2887

On annealed Ni-34.6 at % Al at 1523 K and effects of cooling rates

TIANYI CHENG
Metal Materials Section, Beijing Institute of Technology, P. O. Box 327, Beijing 100081, People's Republic of China, International Centre for Materials Physics, Academia Sinica, Shenyang 110015, People's Republic of China

The microstructures and room temperature mechanical properties of melt spun Ni–34.6 at % Al annealed at 1523 K for 2 h and cooled at different rates were studied. The annealed microstructures and bend ductility were sensitive to the cooling rate. The distribution and relative content of Υ' precipitation were important factors for enhancement of bend ductility of the annealed ribbon. The best bend ductility of the annealed ribbon reached 7.6%, which was considerably better than the as-melt spun ribbon. The emission and transmission of dislocations from ductile Υ' into β to satisfy the need of deformation compatibility played a key role in the improvement of the ductility.

1. Introduction

The intermetallics with many unique properties that make them candidates for high temperature structural application have stimulated much interest in recent years. NiAl with a B2 ordered structure possesses many attractive characteristics, which include a rather high melting temperature (1911 K), low density (5.95 g cm^{-3}) for stoichiometric NiAl, excellent oxidation and sulphidation resistance and good heat conductivity [1, 2]. However, NiAl also has low ductility (< 2%) and poor fracture toughness (4–8 MPa $m^{1/2}$) at room temperature (RT), which blocks its application. In order to improve the mechanical properties at RT, various studies on NiAl–Ni_3Al two-phase alloys [3–5] in addition to the other routes, such as refining grain size [6], microalloying in single crystal NiAl [7], have recently been reported.

Ni_3Al possesses a much higher toughness (about 20 MPa $m^{1/2}$) [8] than NiAl although Ni_3Al without the addition of the boron exhibits low ductility at RT. In addition, precipitation of Ni_3Al (Υ') in NiAl can improve the ductility and toughness of the NiAl-based two-phase alloys [4–5]. However, the mechanisms responsible for the increased properties with Υ' addition have not been clearly defined. It is evident that the Ni_3Al only precipitates in nickel-rich NiAl rather than stoichiometric NiAl, according to NiAl phase diagram [9]. Studies relating characteristics of Υ', such as the morphology, distribution, relative content and size of the precipitates, to heat treatment details have received little attention but it is believed that these characteristics closely control the ductility and toughness of NiAl–Ni_3Al alloys.

In this paper, the microstructures and mechanical properties at RT of melt spun Ni–34.6 at % Al ribbon annealed at 1523 K for 2 h and cooled at different rates are investigated. The effects of the cooling rate on formation, appearance, distribution, relative content and size of Ni_3Al precipitation are also studied. The possible mechanism responsible for the improvement of ambient ductility and toughness of the NiAl alloy as affected by the Ni_3Al precipitation is discussed.

2. Experimental procedure

The nickel-rich ribbon was fabricated by a melt spinning technique, the details of which have been introduced elsewhere [6]. The accurate composition of the ribbon was examined using a traditional chemical analysis method and was found to be Ni–34.6 at% Al [6]. The average thickness of the annealed ribbons was 20.8 μm. The ribbons were carefully sealed under a vacuum of better than 1.333 Pa into a quartz tube and then annealed at 1523 K for 2 h. The different cooling routes, including cooling in different furnaces (small and large), in air and quenching in flowing water with room temperature, were taken. The average cooling rate was estimated according to the furnace temperature and time spent in cooling to RT. The heat treatment details of different samples are outlined in Table I. The microstructures of annealed ribbons were examined by means of Shimazu XD-D1 X-ray diffractometer (XRD) with CuK_α at 40 kV and 20 mA, JEOL JSM-6400 and Hitachi S-570 scanning electron microscopes (SEM) and Jeol 2000FX transmission electron microscopes (TEM). The analysis accuracy of the XRD method is about 0.1 vol % since a monochromatic filter was used in the XRD. In addition to using the same operating parameters, the full scales were adjusted when each XRD pattern of different ribbons was plotted so that the maximum intensity of the peaks in each pattern was the same. In that case, the diffraction intensity of relevant peaks of different ribbons can be compared to obtain qualitative information related to phase transformations

TABLE I Heat treatment details of Ni–34.6 at % Al heated at 1523 K

Ribbon	Hold time (h)	Cooling type	Average cooling rate (K min^{-1})
N1	2	in a large furnace	1.5
N2	2	in a small furnace	10
N3	2	in air	40
N4	2	in flowing water	250

occurring during annealing. The average grain size and relative content of phases were determined by means of a linear intercept method in SEM micrographs. The microcompositional analysis of different phases was performed using an energy dispersive spectrometer (EDS) in SEM and TEM. A standard sample was employed to reduce the average error to less than 5 at %. The room temperature mechanical properties of the annealed ribbon were studied by bend ductility tests [6], which has commonly been applied for measuring the ductility of melt spun ribbons and Vickers microhardness tests. The fracture surfaces were examined using SEM.

3. Results

3.1. Microstructures

3.1.1. XRD analysis

Fig. 1 shows the XRD patterns of annealed ribbons with different cooling rates compared to that for the un-heat treated melt spun ribbon (N0). The diffraction peaks were identified according to the relevant ASTM cards. Comparing with the Ni–Al binary phase diagram [9] (Fig. 2), it can be seen that the N1 consisted of β and Υ' phases, which is close to the equilibrium state although no diffraction peak from the equilibrium Ni_5Al_3 was observed within the limitation of the XRD resolution. The fact is consistent with the report [10] that formation of Ni_5Al_3 is normally difficult and needs annealing for a very long time in an appropriate temperature range. However, we also recently found diffraction peaks contributed by Ni_5Al_3 between 480 °C and 560 °C holding for a short time during heating in an *in situ* study of Ni–34.6 at % Al employing a high temperature X-ray diffractometer (HTXRD) [11]. The actual reasons for the different results and the discrepancy on the equilibrium phase diagram have not been elucidated so the formation kinetics of Ni_5Al_3 need further study. The XRD pattern of N1 (Fig. 1) also indicates that the cooling in the large furnace (cooling rate about 1.5 K min^{-1}) is slow enough not only to allow sufficient precipitation of Ni_3Al (Υ') from NiAl (β) at higher temperature (Fig. 2) but also to suppress the martensitic transformation of β at lower temperatures since no diffraction peak of martensitic NiAl (M-NiAl), as a major phase in melt spun Ni–34.6 at % Al [6], was found in the XRD pattern of N1.

Comparing the XRD pattern of N2 with that of N1, it is evident that the cooling rate in the small furnace (cooling rate about 10 K min^{-1}) is rapid enough to reduce the diffraction intensity of Υ' peaks (see peak

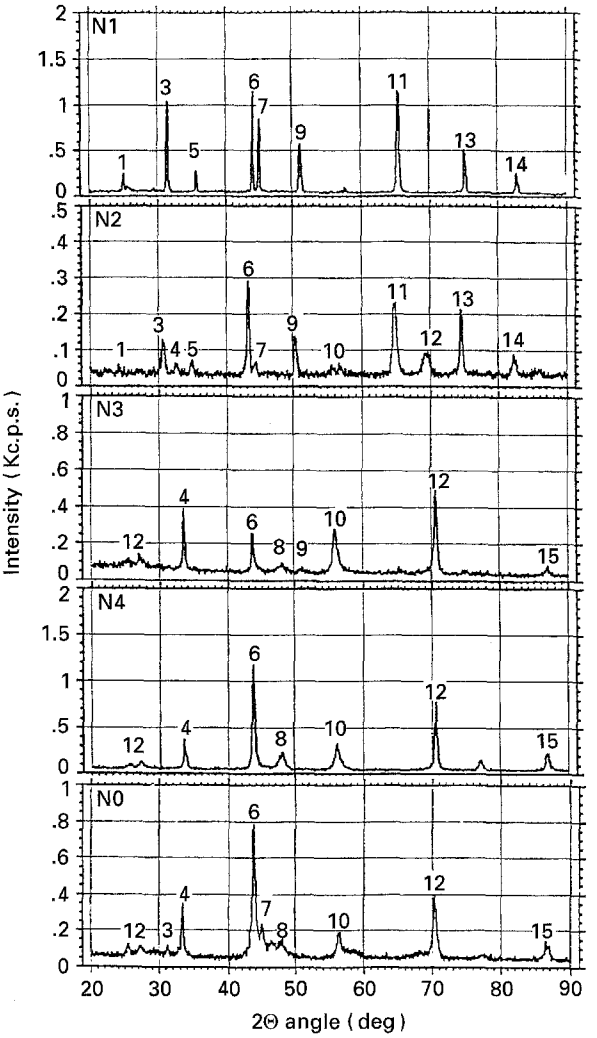

Figure 1 XRD patterns of melt spun and annealed Ni–34.6 at % Al with different cooling rates 1 Υ' (100); 2 M (001); 3 β (100); 4 M (110); 5 Υ' (110); 6 Υ' (111); M (111); 7 β (110); 8 M (200); 9 Υ' (200); 10 Υ' (210), M (201); 11 Υ' (211), β (200); 12 M (220); 13 Υ' (220); 14 β (211), Υ' (300); 15 M (311); M: M-NiAl.

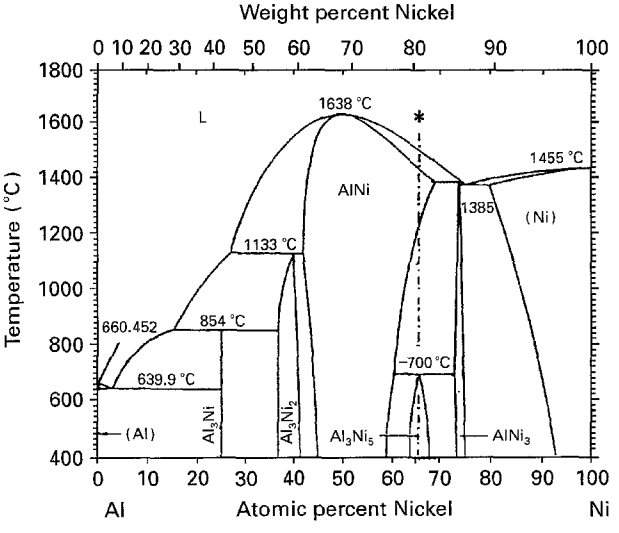

Figure 2 Ni–Al phase diagram [9] (the dot-dash line indicates Ni–34.6 at% Al).

Υ' (100), Υ' (110) and Υ' (200)), suggesting that Υ' precipitated incompletely. Moreover, most of the β transformed into M-NiAl at a lower temperature (M_s of Ni–34.6 at % Al is about 350 °C according to

[12]) during the cooling so the diffraction intensity from β decreased dramatically (see peak β (1 1 0) and β (1 0 0)). Hence, it can be deduced that the critical cooling rate for martensitic transformation in Ni–34.6 at % Al should be about 10 K min^{-1}, which is not very fast compared to the quenching rate for the normal martensite formation. The fact indicates that the martensitic transformation of β in nickel-rich NiAl is rather easy, which is consistent with the observation in the cast Ni–34.6 at % Al [6].

It can still be seen from Fig. 1 that the diffraction peaks of β and Υ' in XRD patterns of samples N3 and N4 cooled at higher rates were almost not present at all. In the XRD pattern of N3, only very weak peaks from Υ' (see peak Υ' (1 0 0), Υ' (2 0 0)) and β (see peak (1 0 0)) were present in addition to strong peaks of M-NiAl. The diffraction peaks in N4 were almost all contributed by M-NiAl except a weak peak of Υ' (1 0 0). Hence, the critical cooling rate to suppress Υ' precipitation during annealing should be about 250 K min^{-1}. When the cooling rate was increased further in the melt spun ribbon (N0), the martensitic transformation of β was partly suppressed since some diffraction peaks of β remained, which was also observed in melt spun nickel-based superalloys [13]. In addition, the Υ' and β in those ribbons are all ordered subsequently Υ' (1 0 0), Υ' (1 1 0) and β (1 0 0) as superstructural diffractions were present.

3.1.2. SEM examination

Figs 3 and 4 show the microstructures of each ribbon observed by SEM at low and high magnification, respectively. It can be seen that ribbon N1 consisted of

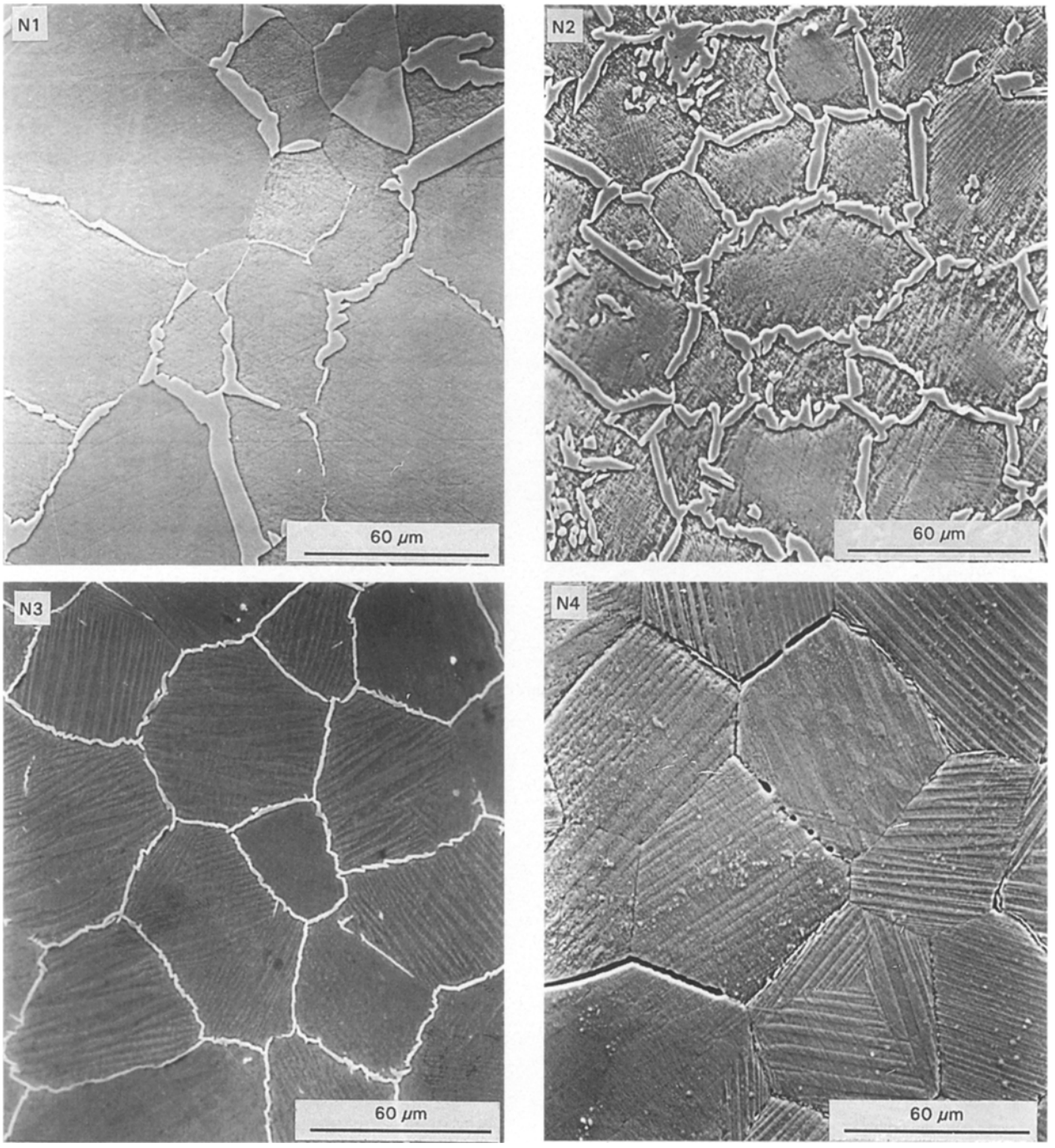

Figure 3 SEM micrographs at lower magnification of microstructures of annealed ribbons with different cooling rates.

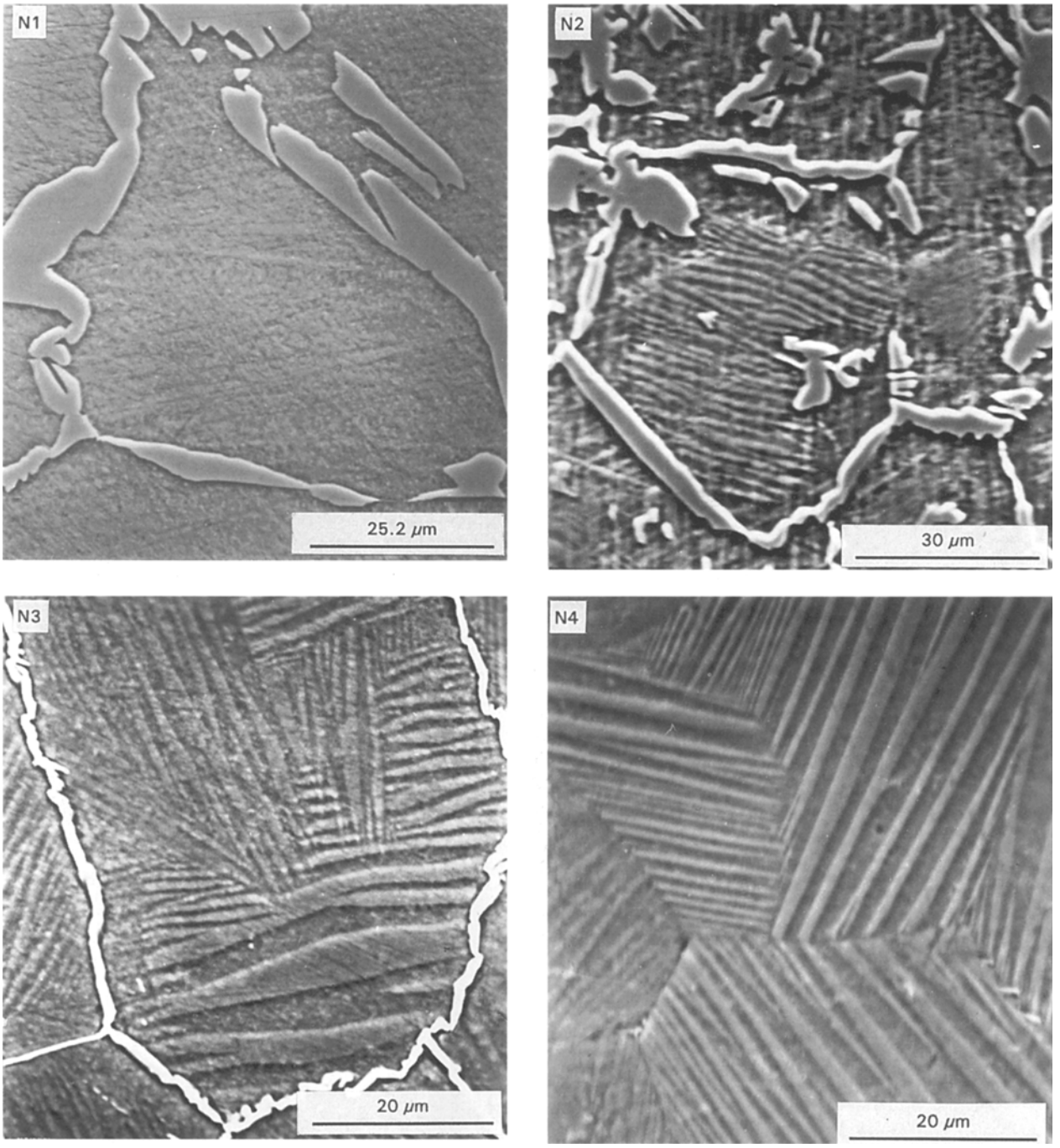

Figure 4 SEM micrographs at higher magnification of microstructures of annealed ribbons with different cooling rates.

β with irregular grain morphology and Υ' located mainly on the grain boundaries of β, the phase constitution of which is consistent with the XRD analysis. The average grain size of β was 51.2 μm. The relative content of Υ' was about 20%, which is smaller than that of prediction based on the Lever rule applied in the (β + Υ'') two-phase field of the Ni–Al phase diagram (Fig. 2). One possible reason for the discrepancy is that the cooling rate of N1 during annealing was not slow enough to allow the sufficient precipitation of Υ'. The other possibility may relate to the phase diagram, since a similar experimental result on the change of relative constitution during heating and cooling in the present alloy employing HTXRD, that was inconsistent with the slope of β/(Υ' + β) phase boundary of the Ni–Al phase diagram, was also found [11]; hence, further study would be necessary. The distribution of Υ' is not completely continuous on the grain boundary of β. The appearance of Υ' also is irregular, strip-like or block-like and the average width of the strip-like Υ'' is about 10 μm.

The Υ' in ribbon N2 formed a "necklace" structure which was present mainly as a film continuously surrounding grains of the matrix. The distribution of the Υ'' on the grain boundary of the matrix was rather uniform and the width of the Υ' film was about 6 μm. The amount of Υ' is smaller than that in N1 and the relative content of Υ' was about 15%, which indicates the incomplete precipitation of Υ' and also coincides with the XRD examination. The grains of the matrix with a irregular polygon-like morphology consisted of M-NiAl as a major phase and minor β. The average

grain size of the M-NiAl was 47.8 μm. Many striations, parallel or intercrossing, which may be traces of stacking faults or twins, as substructures of M-NiAl [6], were present. A few β phases located close to grain boundaries between Υ' film and M-NiAl (Fig. 4), which was discussed in detail in another paper [14]. The average aluminium content of M-NiAl, Υ' and β were 35.2 at % Al, 29.1 at % Al and 39.4 at % Al, respectively. In addition to the present work, the annealing of the same ribbon at 1523 K in the small furnace for 1 h was also performed [14]. The microstructures of the annealed ribbon were very similar to that of N2 except for small differences in the relative content of each phase and smaller grain size. We will not distinguish the results of those two ribbons in the present paper.

As shown in Fig. 3, the Υ' in N3 also formed an almost continuous "necklace" structure with more uniform width but the width of the Υ' film was much narrower than that in N2, only about 2 μm. Comparing with N1, the size and appearance of the Υ' film in N3 suggests its insufficient growth. The relative content of Υ' in N3 was about 6%. A few β were still located in the same area as that in N2 observed by TEM, although it is not obvious in Fig. 4 because of the small content. The grains of M-NiAl consisted of many, almost parallel, thin plates or divided into several intercrossing colonies with different orientations. The plate actually consisted of many parallel and very thin plates again (Fig. 4). The morphology of the M-NiAl in N3 is not similar to that in melt spun ribbon [6], which will be studied further. The average grain size of M-NiAl was 45.4 μm.

In ribbon N4, only very few Υ' phases with an appearance of a discontinuous and very thin line (about 0.2 μm wide) were present on some grain boundaries of M-NiAl (Figs 3 and 4). It is difficult to find any trace of β. The M-NiAl grain with a regular polygon-like appearance consisted mainly of parallel plates. The average grain size of M-NiAl was 44.1 μm. It should be noted that many cracks occurred on the grain boundaries of M-NiAl, which formed perhaps due to severe impingement without the buffering of the ductile Υ' film during the growth of the M-NiAl plates. As pointed before, the above examination by means of SEM is reasonably consistent with the analysis using XRD mentioned in section 3.1.1.

3.1.3. TEM examination

Among the ribbons cooled at different rates, the N2 with good ductility (see section 4.1) was chosen to study the microstructures in detail by means of TEM. Fig. 5(a) shows microstructures observed using TEM. The minor β was located between Υ' and M-NiAl and had a "tweed" appearance. The morphology was similar to that in melt spun superalloys [13,15] but without obvious diffuse streaks in selected area electron diffraction (SAED) patterns (Fig. 7 (c)). The compositions of Υ', β and M-NiAl analysed using EDS in TEM were reasonably consistent with the results examined employing EDS in SEM. The M-NiAl had a special appearance and consisted of a lot of fine striations, which was different from that with a substructure of twins in the melt spun ribbon [6]. The preliminary SAED analysis indicates that the M-NiAl in Fig. 5 (a) was a 4H martensite with a long period stacking ordered structure [16] rather than a normal 3R martensite in nickel-rich NiAl with $L1_0$ structure [17], which will be discussed in a future paper. The Υ' was present with an ordered structure (Fig. 5 (b)), which was the same as shown in the XRD pattern (see section 3.1.1). A lot of dislocations in Υ' with a main appearance of superlattice dislocations, tangles and pile-ups ahead of the interface between β and Υ' were observed (Fig. 6(a)). The difference in the structure and lattice constant between Υ' (face centred cubic (f.c.c.) ordered, $a_0 = 0.365$ nm) and β (body centred cubic (b.c.c.) ordered, $a_0 = 0.288$ nm) are rather large. Hence, in addition to the thermal stress, the stress on phase transformation resulted from the strain may be a reason to produce so many dislocations in Υ' during its precipitation. In particular the precipitation of Υ' occurred in a higher temperature range, above 850 °C for the ribbon according to the study employing HTXRD [11], in which the ductility of the Υ' is very good. In any case, this fact suggests that the Υ' with many mobile dislocations in N2 is ductile at RT although without addition of boron.

On the other hand, many dislocations can also be seen in the normally brittle β at RT (Fig. 6(b)), including many inclined dislocations in the side of β on the interface between β and Υ' (Fig. 6(c)) due to the misfit between them. The interface was not coherent based on the SAED analysis and may be semicoherent. The detailed analysis of the dislocations will be performed further. Only a few interface dislocations were found between β and M-NiAl (Fig. 5(a)), probably due to the larger structural differences. Compared to the β with a low dislocation density in the melt spun ribbon, the observation suggests that the dislocations in β of the annealed ribbon may be related to the high dislocation density in Υ'.

Further investigation proved this presumption. The generation and transmission of dislocations from Υ' into β were found around the interface (Fig. 7(a)) although the origin or kind of dislocation source was not clear. In addition, some dislocations on the interface between β and Υ' moved through the interface dislocations and transmitted into β (Fig. 7(b–d)). The generation and transmission or emission of dislocations may result from the deformation compatibility between Υ' and β. When an external stress, such as a thermal stress during heating and cooling resulting from the difference of thermal expansion coefficients between β and Υ', was applied in a sample the ductile Υ' was easier to deform first. The localized deformation must be constrained by the neighbouring brittle β so the dislocations in Υ' would tend to slip towards β, which led to dislocation pile-ups ahead of the interface between β and Υ'. The stress concentration in the side of the Υ' on the interface would drive the dislocations ahead of the interface to cross through interface dislocations and to move into β. The stress can also operate some potential dislocation sources close to or on the interface between β and Υ' and make the

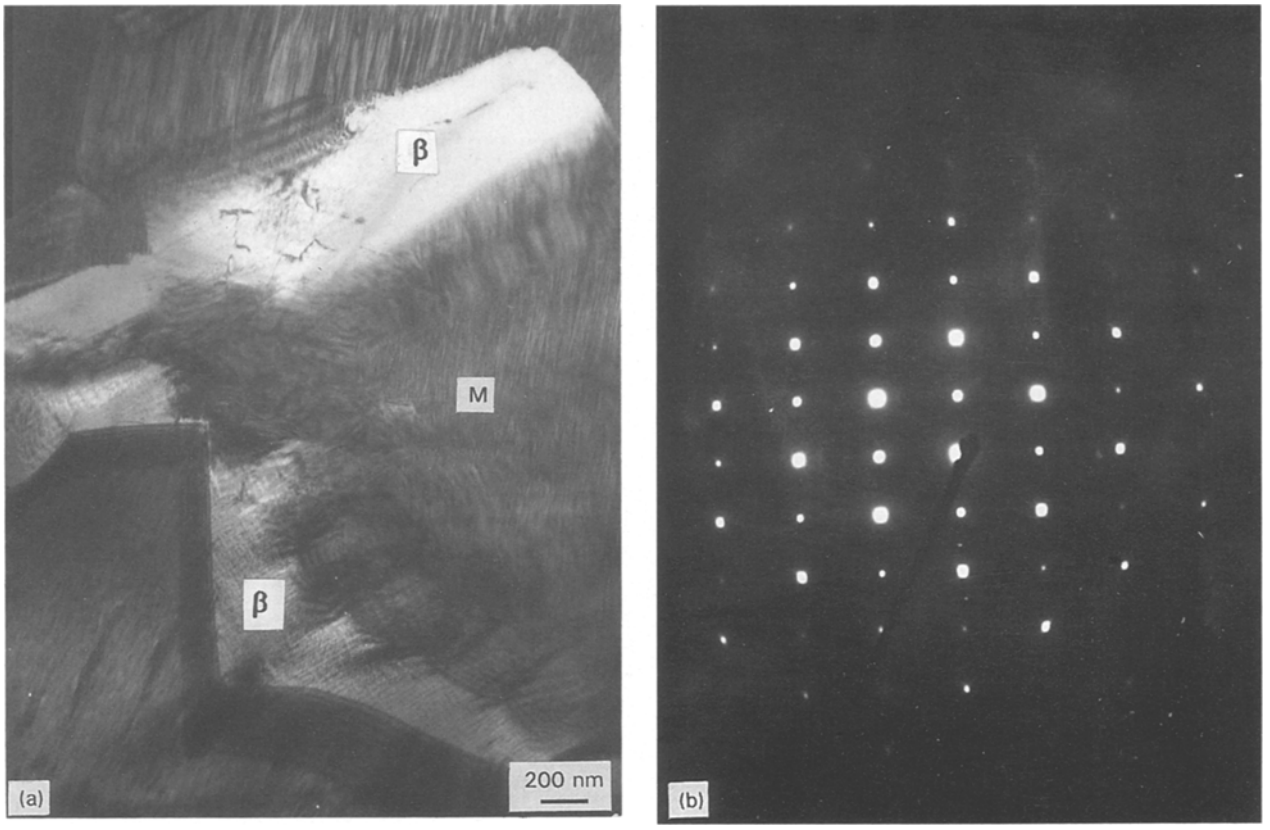

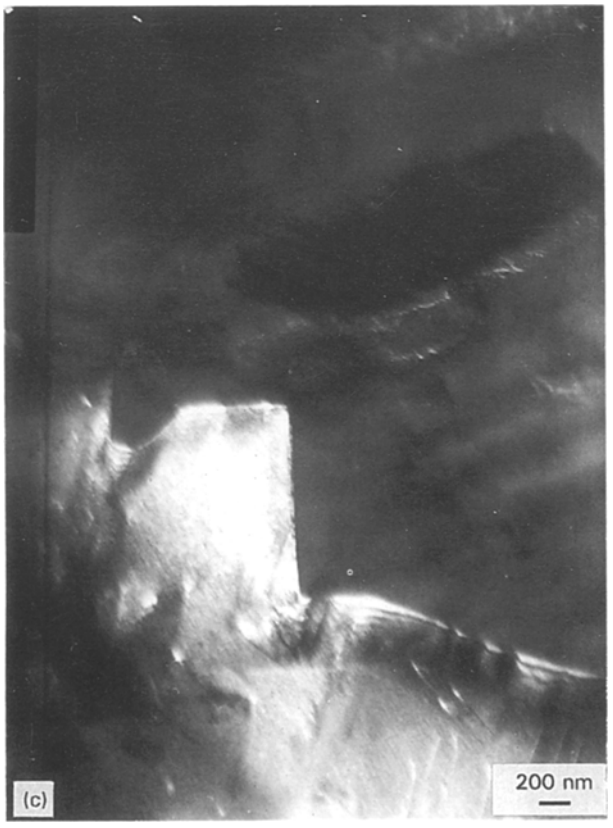

Figure 5 TEM micrographs of microstructures of ribbon N2. (a) Bright field; (b) SAED pattern of Υ', [0 1 1] zone; (c) dark field of Υ' in (a).

dislocation move into β to relieve the stress concentration. Actually, the concept of the interface in two-phase materials to act as a source of dislocations has been theoretically demonstrated [18]. A similar result was also observed in NiAl-based alloys [5]. The increase of the amount of mobile dislocations in the β must improve its ductility very much since the brittleness of the β relates to the lack of sufficient mobile dislocations [1]. The similar dislocation transmission process in M-NiAl of the ribbon N2 has not yet been observed. However, the emission and transmission of dislocations from the interface between Υ' and M-NiAl have already been observed by Noebe *et al.* [5]. The indirect contact with Υ' and the neighbouring β being not so ductile may be the reason for leading to the different situation in M-NiAl of the ribbon N2.

3.2. Mechanical properties

3.2.1. *Bend ductility*

For comparison of the results of the annealed ribbons with that of melt spun ribbon, a 10-mm length of the sample for bend testing was also chosen. The bend ductility of the annealed ribbons was closely associated with the cooling rates and microstructures. The ribbon N4 produced at the highest cooling rate, which consisted almost entirely of M-NiAl, was very brittle and the bend ductility was about zero, which is less than 1.8% of the melt spun ribbon [6]. The result is not surprising since the grain size of M-NiAl in N4 (44.1 μm) was much larger than that of melt spun ribbon (2.2 μm) and the predicted critical grain size for transition from brittleness to ductility was 2.8 μm [19], so the mechanism of refining grain size or increasing interface density [20] could not work. In addition, the intergranular crack after annealing (Fig. 3) also was an important factor to lead to brittleness of N4.

The bend ductilities of ribbons N2, N1 and N3 were 7.6, 6.9 and 5.1%, respectively, which are all

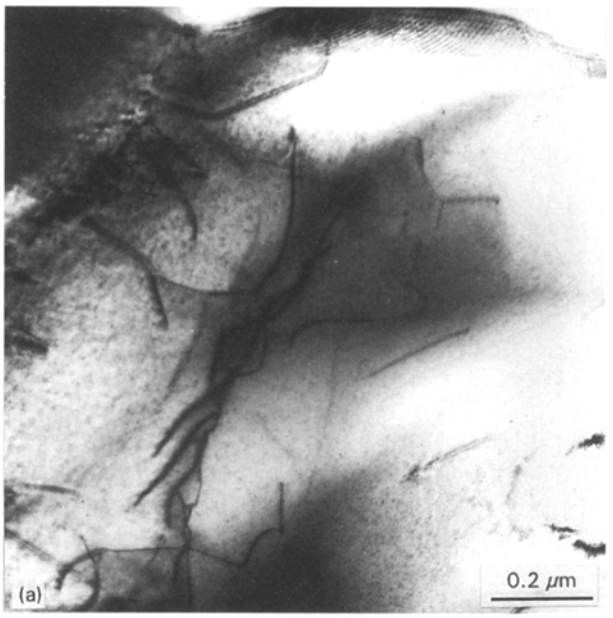

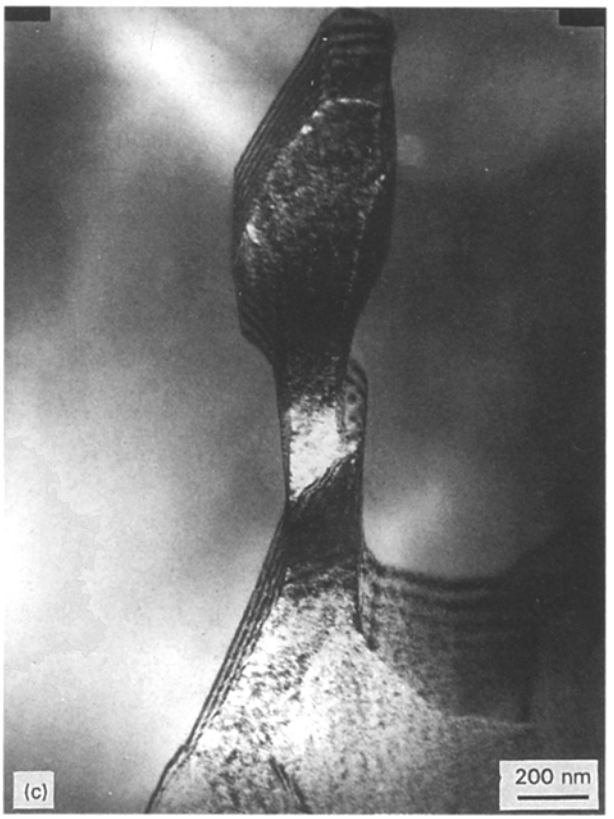

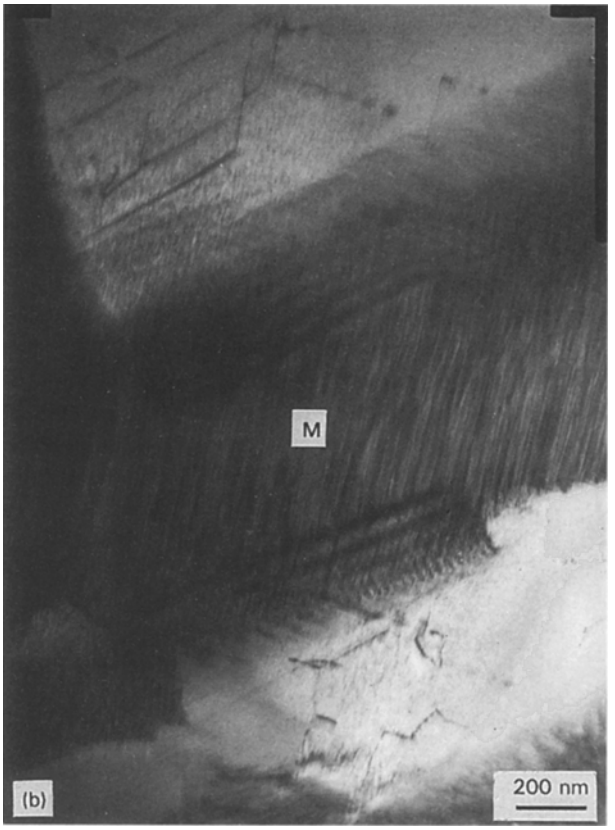

Figure 6 TEM micrograph of dislocations in ribbon N2. (a) Dislocations with high density in Υ'; (b) dislocations in β; (c) inclined dislocations in the side of β on the interface between β and Υ'.

considerably improved in comparison with that of the melt spun ribbon. Since those ribbons all consisted of two or three phases including Υ' phase, it is evident that the ductile Υ' with high density of dislocations and introducing the interface between Υ' and β which could emit or transmit dislocations into β played a key role in enhancement of ductility of the ribbons based on the examination of microstructures in N2. The results are basically consistent with the similar study in a β–Υ'–Υ (Ni) three-phase Ni–30 at % Fe–20 at % Al [21] and annealed melt spun Ni–31 at % Al–18 at % Co alloy [4]. The bend ductility of the annealed NiAlCo ribbon (6.7%) also was very high although a detailed analysis of the mechanism was not performed. In addition, adding a lot of Fe or Co must decrease the melt temperature and increase the density of the NiAl-based alloy, which would be offset against the advantage of improvement of the ductility.

On the other hand, because of difference in the relative content, appearance and size of Υ' in those ribbons, their bend ductilities were different. It can be seen from Table II that the magnitude of grain size of the matrix and the width of Υ' film or line in each ribbon are not important for the bend ductility over the present range. Which phase (β or M-NiAl) is the major matrix phase also does not seem to be very important. The appearance of Υ', particularly whether the film is distributed continuously and homogeneously on the grain boundaries of the matrix, is a key factor for the ductility. The relative content of Υ' phases is also important for enhancing the bend ductility. Hence, the bend ductility of N1 with the most Υ' was not best in the ribbons because it was not very uniform and was discontinuously distributed on the β grain boundaries. On the other hand, in the ribbon N3 Υ' phases were basically continuous and homogeneous on the grain boundary of the matrix but it exhibited bend ductility less than N1 due to much smaller relative content of Υ'. The ribbon N2 had the highest ductility, because it had a microstructure combining a continuous and uniform distribution, and higher relative content of Υ'. The samples of N2 can be severely bent and cycled several times without fracture as shown in Fig. 8. It is possible that the emission and transmission of dislocations from the Υ'

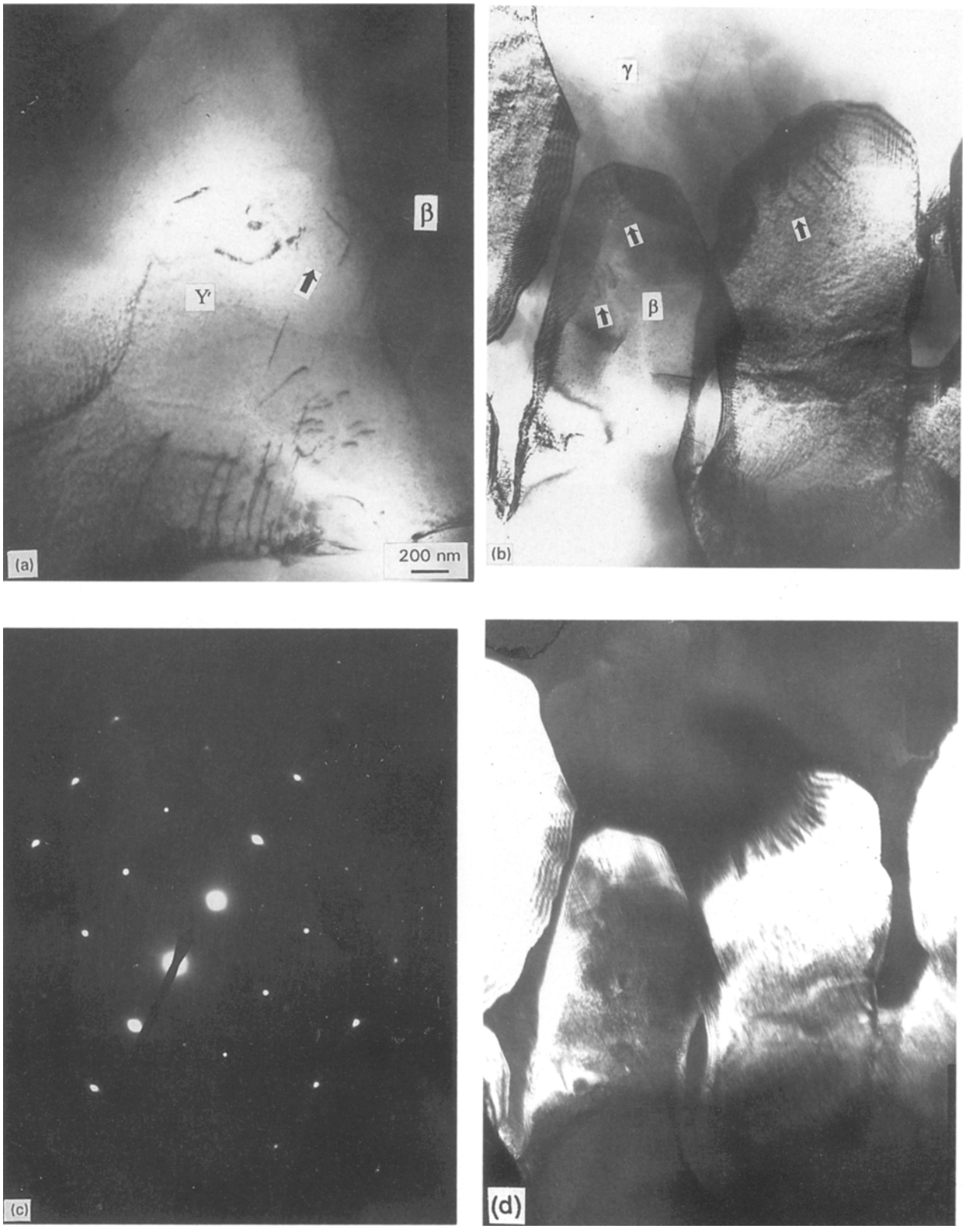

Figure 7 TEM micrographs of emission and transmission of dislocations in ribbon N2. (a) Dislocation generation and emission from γ' into β; (b) dislocation transmission from interface between γ' and β into β (bright field); (c) SAED pattern of β, [1 2 3] zone (d) dark field of β in (b).

film surrounding continuously and homogeneously the brittle phase (β or M-NiAl) can improve the ductility of the brittle phase and best meet the need of deformation compatibility in the ribbon. In the opposite situation, the stress concentration is easy to occur in the site of the brittle phase without contacting with γ' film and would lead to initiation of the crack, as in the cracks on the grain boundaries in N4 shown in Fig. 3. In addition, higher relative content of the ductile γ' can provide sufficient mobile dislocations to emit or transmit, which also is important to improve the ductility of the alloy. It is necessary to prove the deduction related to the mechanism of improvement of the ductility in the ribbons through more detailed work.

TABLE II The relation between microstructures and bend ductility δ of annealed ribbons

Ribbon	d[a] (μm)	n[b] (%)	Morphology of Υ'	Size[c] of Υ' (μm)	δ (%)
N1	51.2	20	strip-like, block-like	10	6.9
N2	47.8	15	necklace-like	6	7.6
N3	45.4	6	necklace-like	2	5.1
N4	44.1	< 1	discontinuous fine line	0.2	0

[a] *d*, grain size,
[b] *n*, relative content of Υ'.
[c] refers to the width of the Υ' film.

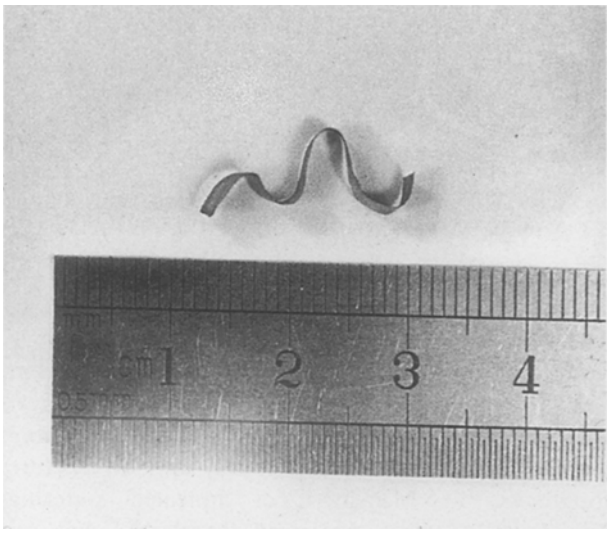

Figure 8 The severely bent sample of the ribbon N2 without crack.

3.2. Microhardness

The effects of the cooling rate on the microhardness of the β, Υ' and M-NiAl in annealed ribbons was not obvious, which is reasonable since the microstructures of each phase could not change much during the cooling with not very fast rates. The average microhardness of Υ', β and M-NiAl were 279, 351 and 442 $kg\,mm^{-2}$, respectively, which is opposite to their relative magnitudes of ductility. The microhardness of the β and M-NiAl also were almost the same as that in the melt spun ribbon [17].

3.3. Toughness

The toughness of the annealed ribbon was not measured because of limitation of the specimen size. However, in addition to the good ductility, the investigation of microcrack propagation and bent fracture surface suggests that the annealed ribbon had good toughness at RT except for the brittle ribbon N4, mentioned before.

Fig. 9 shows two microcracks in bent N2, which propagated intragranularly rather than intergranular growth as a normal route in the cast NiAl [6]. It is evident that the continuous and uniform distribution of the ductile Υ' film on the grain boundary of the matrix was related to the change of the mode of microcrack propagation. Moreover, the microcrack was deflected, twisted and branched, which can reduce the microcrack driving force and enhance the fracture toughness [22]. There also was some shear displacement around the microcrack. The greatest change of the propagation direction occurred when the microcrack met the Υ'. Particularly, the reaction between the microcrack and ductile Υ' led usually to discontinuation of the microcrack (Fig. 9(b)), i.e. stopping

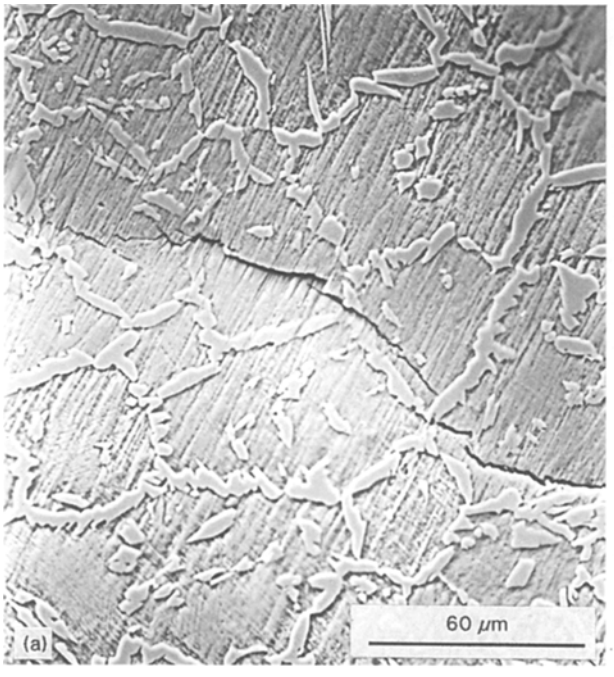

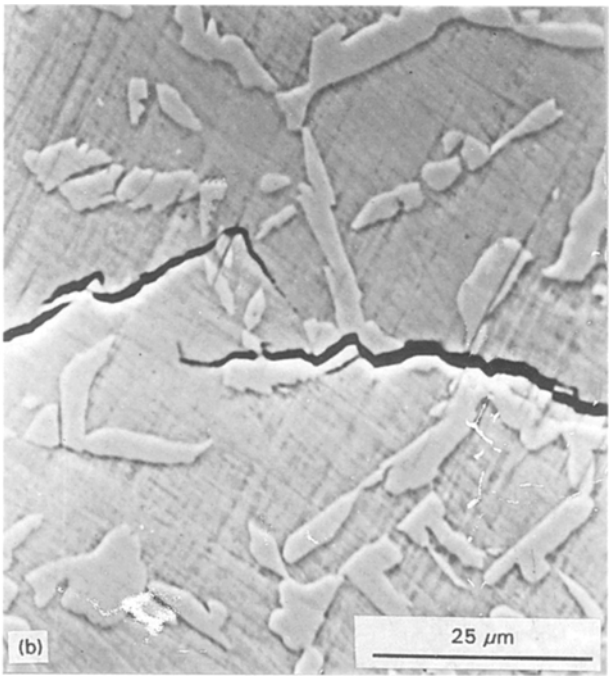

Figure 9 (a), (b) SEM micrographs of microcrack propagation in ribbon N2.

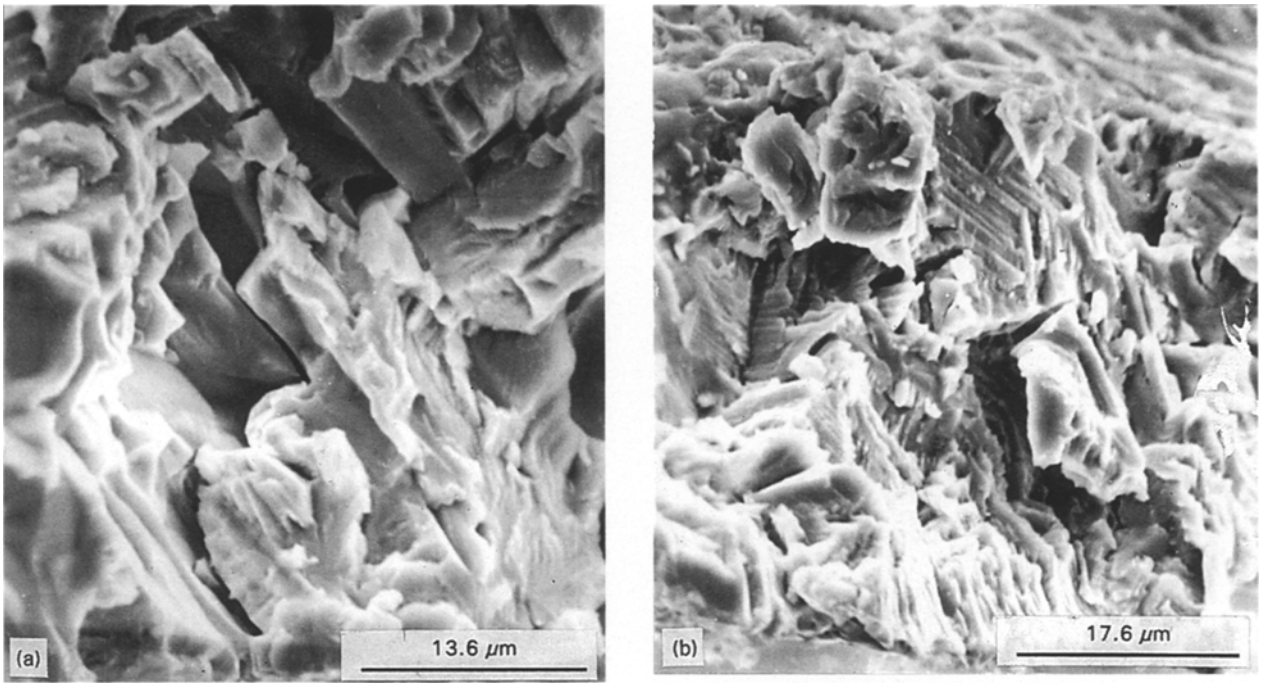

Figure 10 SEM micrographs of bent fracture surface; (a) Ribbon N2; (b) ribbon N3; (c) ribbon N4.

a microcrack and resulting in another microcrack in a different site along a different direction. The facts indicate clearly that the ductile Υ' suppressed effectively the fast and linear propagation of the microcrack which normally occurs in brittle materials. It must produce a means to dissipate fracture energy so that the toughness of the ribbon can be increased.

The observation of the bent fracture surface (Fig. 10) supported this deduction. The fracture surfaces of N2 and N3 all were a mixture of intrafacial and interfacial fracture modes. The ductile part with dimples and the block-like part without deformation trace in Fig. 10(a) correspond to Υ' and M-NiAl in N2, respectively. Many intrafacial microcracks can also be seen in Fig. 10(b), which is evidence for enhanced toughness in brittle materials [23, 24]. Fig. 10(c) shows the fracture surface with a typical intrafacial fracture mode of the ribbon N4 for comparison. The coarse plates of M-NiAl without the obvious intrafacial microcrack can be seen which is different from that of N2 and N3. Hence, the results suggest that the toughness of the annealed ribbons containing ductile Υ' were improved. Actually, a good fracture toughness, 13.5 MPa $m^{1/2}$, of annealed sintering Ni–37 at % Al also containing ductile Υ' was reported [3], which supports our deduction.

Most of all, the ductility and toughness at RT of the annealed Ni–34.6 at % Al ribbons with cooling rate between 1.5 K min^{-1} and 40 K min^{-1} containing the ductile Υ' were considerably improved, in which the interface between Υ' and the brittle phase (β or M-NiAl) played a important role although the interface density was not very high due to grain growth. The results prove again that the different sort of interfaces make different contributions to improvement of the ductility and toughness in brittle materials, such as nickel-rich NiAl [20]. The results also indicate that the cooling rate or cooling route also is important to determine the ductility and toughness of NiAl–Ni_3Al alloy fabricated through annealing.

4. Conclusions

1. Annealing melt spun Ni–34.6 at % Al ribbon at 1523 K for 2 h resulted in different microstructures consisted of ($\beta + \Upsilon'$), ($\beta + \Upsilon' +$ M-NiAl) and (M-NiAl + very few Υ'), respectively, depending on the cooling rate.

2. The critical cooling rate for martensitic transformation of β in Ni–34.6 at % Al is about 10 K min^{-1}, suggesting the martensitic transformation in the nickel-rich NiAl is easier.

3. The relative content, appearance, size and distribution of Υ' precipitation in the annealed Ni–34.6 at% Al was closely related to the cooling rate. The critical

cooling rate for suppressing Υ' precipitation during annealing at 1523 K is about 250 K min^{-1}.

4. The bend ductility at RT of the annealed Ni–34.6 at %Al containing the ductile Υ' was considerably improved in comparison with the melt spun ribbon. However, the annealed ribbon, cooled at a higher rate consisted almost entirely of M-NiAl and was very brittle. The observation of microcrack propagation and fracture surface indicated that the toughness of the ductile ribbons was also enhanced.

5. The improvement of the bend ductility of the annealed Ni–34.6 at % Al depended strongly on the cooling rate or microstructures, particularly the distribution and relative content of the Υ'. The bend ductility of an annealed ribbon with a continuous and uniform Υ' film on the grain boundary of the matrix reached 7.6%. The effects of the cooling rate on the microhardness of the phases were not obvious.

6. In addition to the ductile Υ' phases, the main mechanism responsible for the ductility improvement in the annealed Ni–34.6 at % Al was related to dislocation emission or transmission from the Υ' into the brittle phase (β, possibly M-NiAl) to satisfy the need of deformation compatibility. The interface between Υ' and the brittle phase played an important role in improvement of the ductility and toughness of the annealed alloy.

Acknowledgements

The author thanks the Natural Science Foundation of China for financial support.

References

1. R. DAROLIA, *Journal of Metals Science* **3** (1991) 44.
2. K. S. REUSS and H. VEHOFF, *Scripta Metall.* 24 (1990) 1021.
3. K. S. KUMAR, S. K. MANNAR and R. K. VISWANADHAM, *Acta Metall.* **40** (1992) 1201.
4. D. R. PANK, M. V. NATHAL and D. A. KOSS, *Scripta Metall.* **17** (1990) 519.
5. R. D. NOEBE, R. R. BOWMAN, J. T. KIM, M. LARSEN and R. GIBALA, in "High temperature aluminides and intermetallics", edited by S. H. Whang, C. T. Liu, D. P. Pop and J. D. Stiegler (TMS, Pittsburgh, 1990) p. 271.
6. TIANYI CHENG, *Scripta Metall.* **27** (1992) 771.
7. R. DAROLIA, D. LEHRMAN and R. FIELD, *ibid.* **20** (1992) 1007.
8. J. D. RIGNEY and J. J. LEWANDOWSKI, *Mater. Sci. Eng.* **A149** (1992) 143.
9. T. B. MASSALSKI, " Binary alloy diagram" American Society for Metals, Metal Park, OH, 1986).
10. P. S. KHADKIKAR, I. E. LOCCI, K. VEDULA and G. M. MICHAL, *Metall Trans.* **24A** (1993) 83.
11. TIANYI CHENG and H. M. FLOWER, *Acta Metall.* **42** (1994) 1399.
12. Y. D. KIM and C. M. WAYMAN, *Scripta Metall.* **24** (1990) 245.
13. TIANYI CHENG, and SHOUHUA ZHANG, *J. Mater. Sci. Lett.* **10** (1991) 442.
14. TIANYI CHENG, *Scripta Metall.* **30** (1994) 331.
15. S. M. SHAPIRO, J. Z. LARSEN, Y. NODA, S. C. MOSS and L. E. TANNER, *Phys. Rev.* **B57** (1986) 3199.
16. T. TADAKI and C. M. WAYMAN, *Metallography* **15** (1982) 233.
17. TIANYI CHENG, B. CANTOR, *Mater. Sci. Eng.* **A153** (1992) 696.
18. M. F. ASHBY, in "strengthening mechanism in crystals," edited by A. Kelly and R. B. Nicholson (Wiley, NY, 1971) p. 137.
19. K. S. CHAN, *Scripta Metall.* **24** (1990) 1725.
20. TIANYI CHENG, M. McLEAN and H. M. FLOWER, *ibid.* **26** (1992) 1913.
21. M. LARSEN, A. MISRA, S. HARTFIELD-WUNSCH, R. NOEBE and R. GIBALA, in Proceedings of the Materials Research Society Symposium Vol. 194 (Materials Research Society, 1990) p. 191.
22. K. T. FABER and A. G. EVANS, *Acta Metall.* **3** (1983) 565.
23. J. W. HUTCHINSON, *ibid.* **35** (1987) 1605.
24. TIANYI CHENG, *J. Mater. Sci* **28** (1993) 5909.

Received 15 February
and accepted 4 November 1994